ACS APPLIED MATERIALS & INTERFACES

www.acsami.org

Research Article

KN95 and N95 Respirators Retain Filtration Efficiency despite a Loss of Dipole Charge during Decontamination

Wonjun Yim, Diyi Cheng, Shiv H. Patel, Rui Kou, Ying Shirley Meng, and Jesse V. Jokerst*

Cite This: https://dx.doi.org/10.1021/acsami.0c17333

Read Online

ACCESS | Metrics & More | Article Recommendations | Supporting Information

ABSTRACT: N95 decontamination protocols and KN95 respirators have been described as solutions to a lack of personal protective equipment. However, there are a few material science studies that characterize the charge distribution and physical changes accompanying disinfection treatments, particularly heating. Here, we report the filtration efficiency, dipole charge density, and fiber integrity of N95 and KN95 respirators before and after various decontamination methods. We found that the filter layers in N95 and KN95 respirators maintained their fiber integrity without any deformations during disinfection. The filter layers of N95 respirators were 8-fold thicker and had 2-fold higher dipole charge density than that of KN95 respirators. Emergency Use Authorization (EUA)-approved KN95 respirators showed filtration efficiencies as high as N95 respirators. Interestingly, although there was a significant drop in the dipole charge in both respirators during decontamination, there was no remarkable decrease in the filtration efficiencies due to mechanical filtration. Cotton and polyester face masks had a lower filtration efficiency and lower dipole charge. In conclusion, a loss of electrostatic charge does not directly correlate to the decreased performance of either respirator.

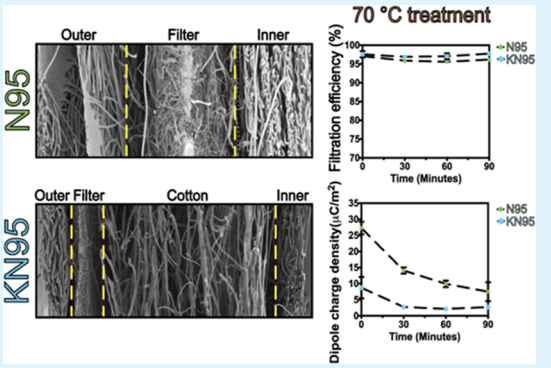

KEYWORDS: *dry-heat, N95 decontamination, sterilization, personal protective equipment (PPE), COVID-19*

INTRODUCTION

The ongoing Coronavirus Disease 2019 (COVID-19) pandemic has had a major impact on human health and society with a mortality rate apparently higher than that of influenza.[1] COVID-19 results from the severe acute respiratory syndrome coronavirus 2 (SARS-CoV-2) infection in which the spike (S) protein on the SARS-CoV-2 plays a key role in mediating viral entry into the human cell.[2] The main routes of transmission between humans are likely aerosols and droplets.[3] When an infected person coughs, sneezes, or speaks, the virus is excreted and dissolved droplets (>5 to 10 μm) or aerosols ($\leq$5 μm) that can remain and travel in the air.[4,5]

N95 respirators have been used to protect wearers against such viral aerosols and droplets. They have at least 95% filtration efficiency for NaCl particles sized 0.1−0.3 μm with even higher filtration efficiency at higher particle size (approximately 99.5% or higher for 0.75 μm particles).[6] Hence, N95 respirators offer excellent protection when they are sealed tightly over the face. Filter fabrics are made of nylon, cotton, polyester (PE), and polypropylene (PP).[7] Nylon filters have good resistance to rubbing, and cotton filters are environmentally friendly. PE filters offer good acid-resistance and excellent durability against elevated temperatures up to 150 °C.[8] PP filters are the lightest among the synthetic fabrics and have good resistance to acids and alkalis.[8] Nonwoven PP fabric is composed of random fibrous webs in which individual fibers are bound together in a random arrangement; thus, the inhaled particles interact with the fibers and adhere efficiently.[9]

Here, we focused on PP, a common material used for the filter layer in the respirators.[10] Spun-bonding and melt-blowing are two key manufacturing processes for fabricating nonwoven PP fabric.[11] Since the diameter of the spun-bond (SB) fiber is larger than that of melt-blown (MB) fiber,[12] SB fibers have been used as the outer or inner layer of the respirators to provide mechanical support for other layers.[13] MB fibers have a high surface area per mass (2 m^2/g), at least 10-fold larger than SB fibers (0.2 m^2/g), and play an important role in the filtration performance.[14] In addition to its high packing density, an electrostatic field applied during the MB manufacturing process induces electrostatic charges within nonwoven MB fibers.[15,16] This field gives the MB microfibers dipole charges on their surfaces, thus improving their filtration efficiencies.[17,18] Therefore, the degree of packing density and the induced electrostatic charge determine the filtration efficiency of nonwoven PP fabric.[19]

Received: September 28, 2020
Accepted: November 18, 2020

Shortages of personal protective equipment (PPE) such as N95 respirators for healthcare workers have been widely reported, especially at the beginning of the pandemic.[20] Unapproved N95 respirators can cause additional risks.[21] Thus, a variety of decontamination methods have been studied to reuse N95 respirators: vaporized hydrogen peroxide (VHP), 70 °C dry-heat, ultraviolet light (UV), and 70% ethanol have all been described to inactivate SARS-CoV-2.[22−24] Although the VHP method is a well-known sterilization technology[25] that has been approved by Food and Drug Administration (FDA),[26] it needs complicated equipment and a trained technician. The ethanol method can damage N95 respirators after the first cycle of decontamination, and UV-radiation has limited penetration through the multiple layers of the respirator.[22] Hence, dry-heat has emerged as a simple, effective, and low-cost decontamination method;[27,28] it uniformly disinfects respirators with good scalability.[29] However, understanding of the physical and electrostatic changes induced by heat treatment remains incomplete.

Hence, we evaluated the effect of decontamination on the respirators and include a special emphasis on KN95 respirators as potential alternatives to N95 respirators with their performance and material science properties. Recent works[7,22,27,28,30,31] focused nearly exclusively on the performance of the respirators, i.e., their filtration performance. Here, we carefully studied both filtration efficiency and dipole charge density. Charge density is related to electrostatic filtration but has not yet been investigated during decontamination. We also investigated fiber integrities of N95 and KN95 respirators before and after dry-heat decontamination.

RESULT AND DISCUSSION

Structural Components of N95 and KN95 Respirators. N95 respirator is a filtering facepiece respirator (FFR) that meets the U.S. National Institute for Occupational Safety and Health (NIOSH) classification with at least 95% filtration efficiency. The 3M 1860, 8210, and 8511 are the most popular N95 models used in the hospitals, and they have three structural components: outer, filter, and inner layers (Figure 1A). Figure 1B shows that the thickness of the filter layer was 3-fold thicker than the outer or inner layers and consisted of more than 50% of the entire layer thickness (Table S1). The fiber diameters of the outer, filter, and inner layers were 27.07 ± 3.64, 2.79 ± 0.95, and 24.46 ± 5.18 μm, respectively (Figure S1A). Therefore, the filter layer had good mechanical filtration: smaller fibers lead to smaller pore-area size[14] (Figure 1C). Furthermore, the dipole charge density imposed on the filter layer was 20-fold larger than the outer and inner layers leading to major electrostatic filtration (Figure 1D).

KN95 respirators follow the Chinese standards.[32] Some of these have similar filtration performance as the N95 respirator but are not NIOSH approved. During the COVID-19 pandemic, the FDA issued an umbrella Emergency Use Authorization (EUA) for KN95 respirators in response to concerns associated with an insufficient supply of N95 respirators. We selected four different brands of commonly available KN95 respirators including the respirators approved by the EUA of FDA (Figure 2A). KN95 respirators are composed of four layers: outer, filter, cotton, and inner layers (Figure 2B). The filter layer of KN95 respirators is at least 8-fold thinner than that of N95 respirators. Less than 20% of the total respirator thickness is due to the filter layer in KN95 respirators (Table S1).

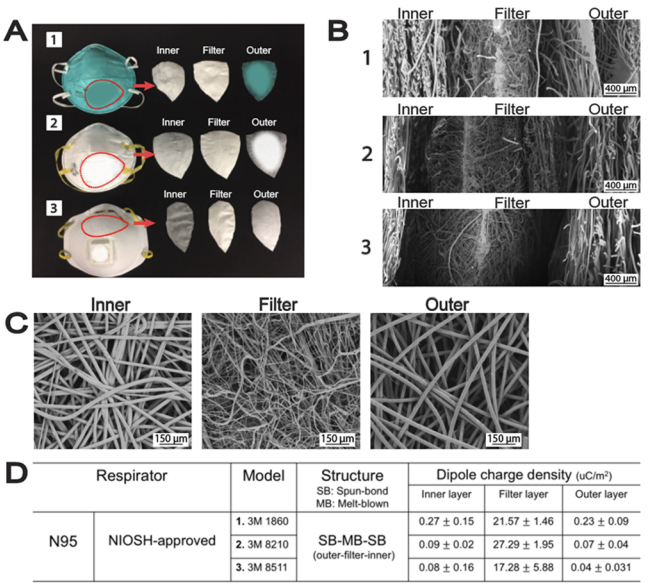

Respirator		Model	Structure SB: Spun-bond MB: Melt-blown	Dipole charge density (uC/m²) Inner layer	Filter layer	Outer layer
N95	NIOSH-approved	1. 3M 1860	SB-MB-SB (outer-filter-inner)	0.27 ± 0.15	21.57 ± 1.46	0.23 ± 0.09
		2. 3M 8210		0.09 ± 0.02	27.29 ± 1.95	0.07 ± 0.04
		3. 3M 8511		0.08 ± 0.16	17.28 ± 5.88	0.04 ± 0.031

Figure 1. Structural components and charge distribution in N95 respirators. (A) 1: 3M 1860, 2: 3M 8210, and 3: 3M 8511. Red-dotted circles and red arrows indicate the part where the mask was removed for analysis. (B) N95 respirators have inner, filter, and outer layers. The filter layer occupies a large portion of the entire thickness. (C) Filter layer has the smallest pore-area size (3M 1860) compared to the inner and the outer layers. 3M 8210 and 3M 8511 are shown in Figure S4A. (D) Most of the dipole charges are imposed on the filter layer and offer electrostatic filtration. The average dipole charge density was calculated from five replicate measurements on five different points on the sample.

Importantly, KN95 respirators had a supplementary layer between the filter and the inner layers, i.e., the so-called "cotton layer" occupying 70% of the respirator.[33] Prior work showed that fibers in the cotton layer have a core−shell structure (Figure S1B) in which the outer shell was made of 95% cellulose and 0.6% natural wax.[34] Here, we used SEM to measure the fiber diameters in the outer, filter, cotton, and inner layers: 26.07 ± 3.63, 3.23 ± 1.28, 22.97 ± 4.12, and 31.07 ± 2.10 μm, respectively (Figure S1B). The filter layer had the smallest pore-area size (Figure 2C). Likewise, the dipole charge density of the filter layer was 8 times higher than that of other layers (Figure 2D). Hence, filter layers in both N95 and KN95 respirators play an important role in mechanical and electrostatic filtration.

In addition to N95 and KN95 respirators, we also investigated cotton, polyester, and surgical masks, which are more easily accessible to the public (Figure S2A,2B). Surgical masks are made of three-layered fabrics including the filter layer. Cotton and polyester masks are composed of two-layered fabrics. Surgical masks had 15% lower filtration efficiency than N95 respirators. Cotton and polyester cloth masks had 70% lower filtration efficiency than N95 respirators (Figure S2C). Surgical masks had some dipole charge on the filter layer, whereas cotton and polyester masks had no dipole charge (Figure S2D). Heat treatment did not markedly affect the filtration efficiencies of surgical, cotton, and polyester masks due to their low baseline values (Figure S2C). The filtration efficiencies seen here are consistent with prior work.[35] All of these materials provide the wearer with some barrier to transmission.[33]

https://dx.doi.org/10.1021/acsami.0c17333
ACS Appl. Mater. Interfaces XXXX, XXX, XXX−XXX

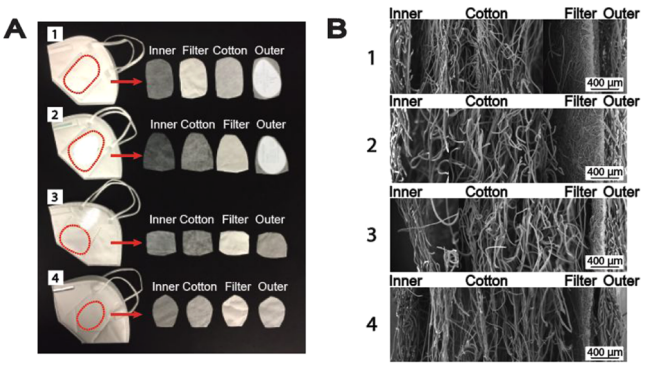

D

Respirator		Model	Structure (SB: Spun-bond, MB: Melt-blown, CT: Cotton)	Dipole charge density (uC/m²) Inner layer	Cotton layer	Filter layer	Outer layer
KN95	EUA approved	1. Decopro	SB-MB-CT-SB (Outer-filter-cotton-inner)	1.24 ± 0.15	0.13 ± 0.01	8.75 ± 3.29	1.88 ± 0.46
		2. Powecom		1.36 ± 0.30	0.01 ± 3.91	9.99 ± 4.56	0.45 ± 0.12
	Non-EUA approved	3. SupplyAID		1.24 ± 0.13	0.02 ± 0.01	16.49 ± 3.49	1.06 ± 0.18
		4. Yomasi		1.41 ± 0.31	0.01 ± 0.004	4.51 ± 1.29	2.65 ± 0.47

Figure 2. Structural components and charge distribution in KN95 respirators. (A) 1: Decopro, 2: Powecom, 3: SupplyAID, and 4: Yomasi. The Decopro and Powecom are EUA-approved KN95 respirators. Red-dotted circles and red arrows indicate the area of the mask that was removed for analysis. (B) KN95 respirators have inner, cotton, filter, and outer layers. (C) Filter layer has the smallest pore-area size than the other layers (Yomasi). Decopro, Powecom, and SupplyAID are shown in Figure S4B. (D) Most of the dipole charges are imposed on the filter layer and offer electrostatic filtration. The average dipole charge density was calculated from five replicate measurements on five different points on the sample.

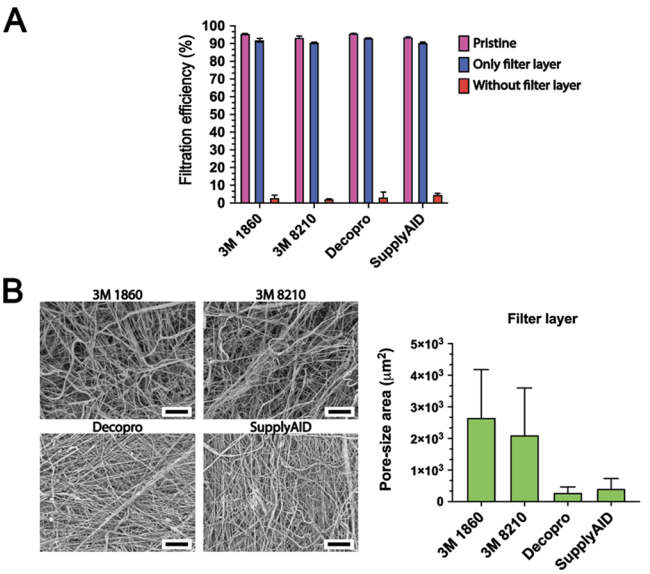

Figure 3. Filtration efficiency and pore-area size of the filter layer. (A) Filtration efficiencies with and without the filter layer. The error bars represent the standard deviation of five measurements. 3M 1860 and 3M 8210 are N95 respirators. Decopro (EUA-approved) and SupplyAID (non-EUA-approved) are KN95 respirators. (B) Scanning electron microscopy (SEM) images show that KN95 respirators have a 10-fold smaller pore-area size than N95 respirators (see Figure S3). All scale bars represent 150 μm. The error bars represent the standard deviation of 20 measurements.

As a control, we also measured the filtration efficiencies with and without the filter layer in N95 and KN95 respirators. The filtration efficiencies in both respirators were less than 5% without the filter layers—90% of filtration efficiencies came from the filter layers (Figure 3A). This result indicated that the major function of the other layers is to protect the filter layer and to remove macroscopic particles. Interestingly, the filter layers in EUA-approved KN95 respirators had similar filtration efficiencies as the N95 respirators despite being thinner and having lower dipole charge densities. This might be because EUA-approved KN95 respirators had a 10-fold smaller pore-area size than N95 respirators (Figure 3B); smaller pore-area size can trap more particles.[14]

Respirator Heat Treatment. Particle capture includes five mechanisms such as interception, physical sieving, inertial separation, diffusion, and electrostatic attraction.[36,37] These steps can remove airborne particles on the various layers of N95 and KN95 respirators (Figure S5). The National Institute of Health (NIH) has validated 70 °C treatment to inactivate SARS-CoV-2.[22,38] Therefore, N95 and KN95 respirators were heat-treated in the oven for three cycles (30 min/cycle) at 70 °C. We also conducted 150 °C treatment to evaluate the impact of extreme heating conditions on the material properties as a positive control. Figure 4A,B shows the fiber integrity of each layer in N95 and KN95 respirators after 60 min of 70 and 150 °C treatments. Particles captured on the outer layer were removed by 70 °C heat treatment (Figure 4A). This might be because of a loss of electrical entrapment due to charge dissipation at high temperatures. We also found some structural instabilities when heated at 150 °C. For example, the inner layer of N95 respirators began to melt, leading to fiber linkages with other fibers nearby (Figure S6). The outer layer of KN95 respirators fractured, and balloon-shaped fiber expansions occurred in the cotton layer of KN95 respirators (Figure S7). However, the filter layers of N95 and KN95 respirators had no structural deformations because the filter layers were made of MB fibers, which have high resistance to high temperature.[16] Those structural instabilities occurring at 150 °C demonstrated that 70 °C was a suitable temperature for the dry-heat method.

Filtration Efficiency and Dipole Charge Density After Heat Treatment. We measured the filtration efficiency and dipole charge density of N95 and KN95 respirators after 70 and 150 °C treatments to evaluate the effect of dipole charge density on the filtration efficiency. Although the dipole charge density of the three different N95 respirators decreased after heat treatments (Figure 5B,D,F), there was no significant drop in the filtration efficiencies (Figure 5A,C,E) because filtration efficiency was also affected by mechanical filtration. Mechanical filtration is based on inertia impaction, interception, and diffusion; these are not markedly influenced by the charge.[39] In addition, the increase in filtration efficiency due to electrostatic attraction is most significant for 2−100 nm particles,[40] illustrating that filtration efficiency depends on the particle size and air flow.[41]

Particle size is a key consideration. As a model, we used a lit candle to produce fine particles of black carbon in the air for measuring filtration efficiency. The geometrical mean diameter (GMD) obtained from the steady burning of candles is around 20−30 nm with the larger sizes up to about 150 nm because of aggregation.[42,43] We also took SEM images of N95 samples after the filtration test to measure the particle size attached on

https://dx.doi.org/10.1021/acsami.0c17333
ACS Appl. Mater. Interfaces XXXX, XXX, XXX−XXX

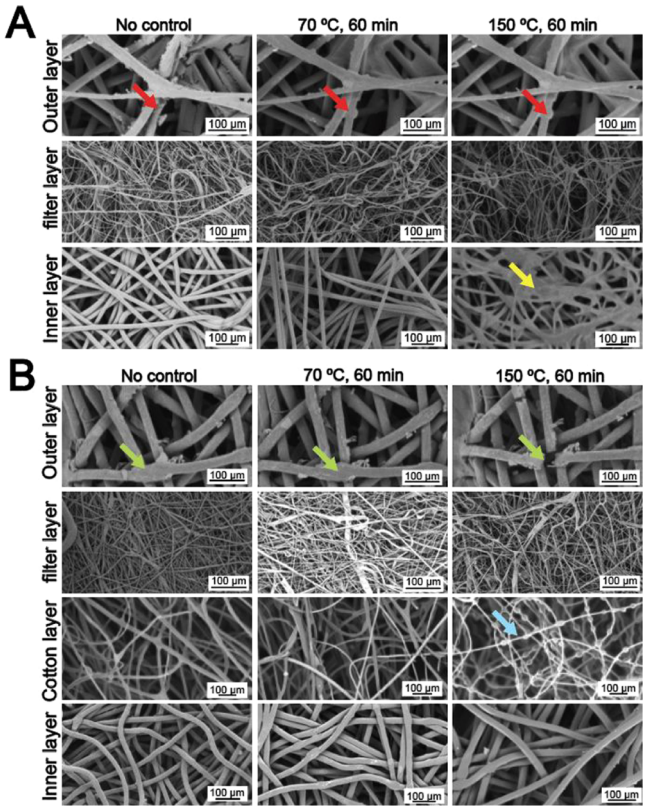

Figure 4. Fiber integrity of N95 (3M 1860) and KN95 (Yomasi) respirators. (A) Red arrows indicate that the particles attached on the outer layer of 3M 1860 are removed after heat treatment. The filter layer has no structural changes, while the inner layer begins to melt when heated at 150 °C (yellow arrow). 3M 8210 and 3M 8511 show similar results (see Figure S6A). (B) Filter layer of Yomasi has no structural deformation; however, a fracture in the outer layer (green arrows) and balloon-shaped fiber expansion in the cotton layer (blue arrow) occur when heated at 150 °C. Decopro, Powecom, and SupplyAID show similar results (see Figure S6B).

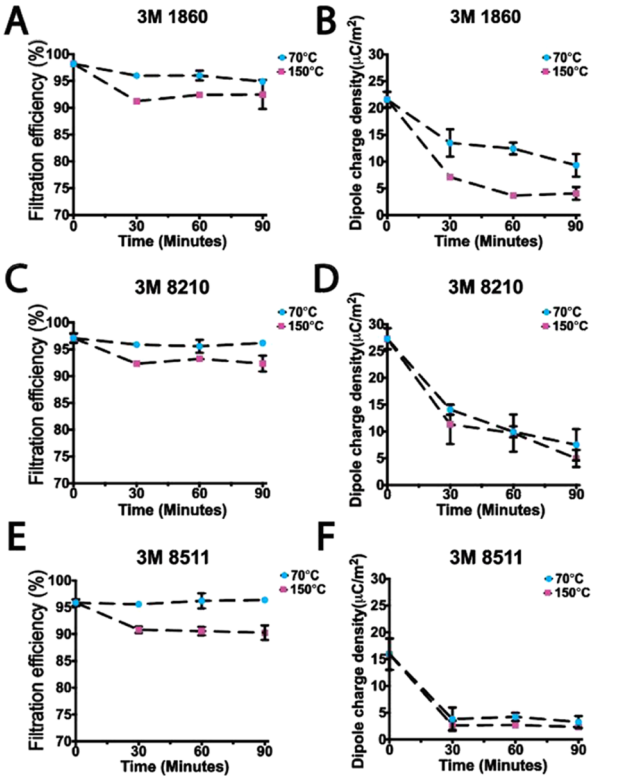

Figure 5. Filtration efficiency and dipole charge density of N95 respirators during heat treatment. Filtration efficiency of (A) 3M 1860, (C) 3M 8210, and (E) 3M 8511. Dipole charge density of (B) 3M 1860, (D) 3M 8210, and (F) 3M 8511. Dipole charge density decreases during heat treatments, but there is no remarkable drop in filtration efficiency. The error bars represent the standard deviation of five measurements.

the fibers. Large particles (5−10 μm in diameter) and small particles (2−1000 nm in diameter) were attached on the outer, filter, and inner layers (Figure S5). Hence, mechanical filtration allowed N95 respirators to retain their filtration efficiencies despite a loss of dipole charge during decontamination.

The filtration efficiencies of N95 respirators remained over 95% after each cycle of 70 °C treatment, while KN95 respirators varied from 80 to 97%. EUA-approved and non-EUA-approved KN95 respirators had at least a 10% difference in their filtration efficiencies (Figure 6A,G). This indicated that not all KN95 respirators are suitable alternatives to N95 respirators. KN95 respirators had similar behavior as N95 respirators. There was a decrease in dipole charge density after heat treatments, but the filtration efficiency remained relatively constant (Figure 6).

The filter layer of N95 respirators had not only an 8-fold thicker thickness but also 2-fold higher dipole charge density at baseline than that of KN95 respirators. Nevertheless, some KN95 respirators showed filtration efficiencies as high as N95 respirators (Figures 5 and 6A,E). This might be because of their small pore-area size of the filter layer and their supplementary cotton layer. Cotton, natural silk, and chiffon were found to provide good protection across the 10 nm to 6 μm particulates.[7] Furthermore, combining cotton layers created hybrid structures that might be an effective way to leverage mechanical and electrostatic filtration.[7]

The dipole charge densities of N95 and KN95 respirators dropped by at least 50% during the first cycle of heat treatment. This charge loss might be because a higher initial dipole charge density induces higher inner electrical field, which results in a faster decay rate of dipole charge density.[44−46] A subsequent decrease in the dipole charge density occurred after each cycle of heat treatment for two reasons. First, the dipolar charges in the polymer material depend on steady-state trapping/detrapping. The detrapping coefficient of electrons and holes is described as $D = \nu^*\exp(-w/k_BT)$, where ν is the attempt to escape frequency and w is the detrapping barrier.[46] With increasing temperature (T), trapped electrons and holes are more easily detrapped. Second, charge transport at the interface between the solid polymer and the air at the boundary follows the Schottky law, which indicates that charge dissipation fluxes become larger at higher temperatures.[44−46]

Humidity can be a natural conductor to facilitate dipole charge dissipation.[47] Thus, the dipole charge density of N95 respirators decreased 70−80% after H_2O_2 treatment (Figure 7A). However, there was no significant drop in the filtration efficiency (Figure 7B). To minimize the effect of electrostatic attraction, we used isopropanol (IPA) to remove nearly all dipole charges[48] in the filter layer (Figure 7C) and measured the filtration efficiency. The filtration efficiencies of N95 respirators after IPA treatment decreased about 7−15% after

https://dx.doi.org/10.1021/acsami.0c17333
ACS Appl. Mater. Interfaces XXXX, XXX, XXX−XXX

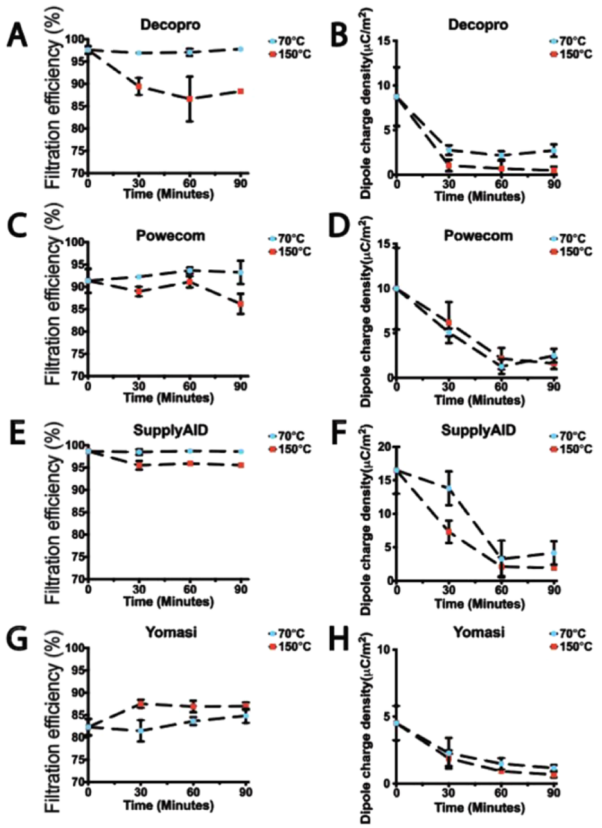

Figure 6. Filtration efficiency and dipole charge density of KN95 respirators during heat treatment. Filtration efficiency of (A) Decopro, (C) Powecom, (E) SupplyAID, and (G) Yomasi. Dipole charge density of (B) Decopro, (D) Powecom, (F) SupplyAID, and (H) Yomasi. A loss of dipole charge occurs during heat treatments; however, it does not directly decrease filtration efficiency. The error bars represent the standard deviation of five measurements.

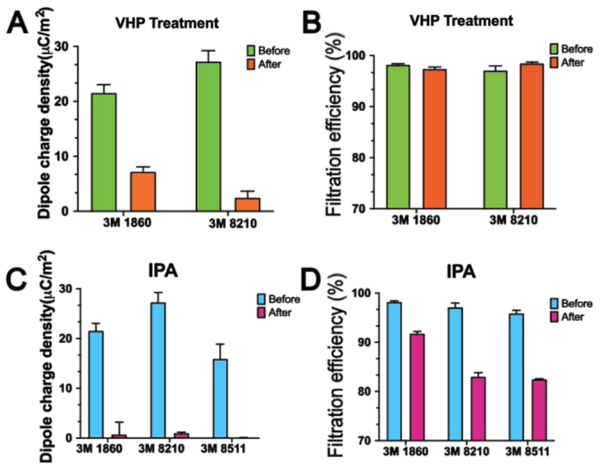

Figure 7. Dipole charge density and filtration efficiency of N95 respirators after VHP and IPA treatments. (A) Loss of dipole charge density occurs after VHP treatment. (B) N95 respirators still have high filtration efficiency after VHP treatment. (C) IPA method completely removes all dipole charges. (D) Filtration efficiencies of N95 respirators before and after IPA treatment. Filtration efficiencies of the charge-free KN95 respirators are shown in Figure S10. The error bars represent the standard deviation of five measurements.

removing all dipole charges. Such decreases in filtration efficiencies indicated that electrostatic charges contributed to the filtration performance. In addition, there was no structural damage on the fiber integrity of the filter layer, and no thickness shrinkage occurred during the IPA drying process in the filter layers of N95 (Figure S8) and KN95 (Figure S9). Charge-free N95 respirators still showed 83−92% filtration efficiency due to mechanical filtration (Figure 7D).

CONCLUSIONS

At the early stages of the COVID-19 pandemic, it was unclear if the global supply chain would be able to adequately respond to the surging demand for PPE. This lack of supply motivated these studies into PPE reuse. In this study, we investigated three N95 respirators, four KN95 respirators, and commonly available commercial masks including the impact of heat-based treatment. We compared their baseline features as well as their physical filtration properties after disinfection via the dry-heat method. Filtration efficiencies of N95 and KN95 respirators remained relatively constant after 70 °C heat treatments. Upon further heating to 150 °C, structural instabilities such as fracturing, melting, and balloon-shaped fiber expansions were found at the outer, cotton, and inner layers. There was no fiber deformation in the filter layer. This indicated that 70 °C was a suitable temperature for the dry-heat method; the filter layer had strong thermal durability.

Dipole charge density was also investigated in this study because electrostatic charge is involved in the filtration performance of respirators.[15,16] In both respirators, large decreases in the dipole charge density were observed after several heat treatments. However, there was no significant drop in filtration efficiency because multiple parameters (i.e., mechanical filtration) were involved in the filtration performance. Furthermore, EUA-approved KN95 respirators had filtration efficiencies as high as N95 respirators, perhaps because of their small pore-area size of the filter layer and their cotton layer. There was no quantitative relationship between dipole charge density and filtration efficiency during decontamination; however, a loss of dipole charge could affect the electrostatic performance.

One limitation of this work is that the particles used for the measurements may not be representative of the aerosols containing viral particles. Thus, the filtration efficiency shown here might not be representative of the filtration of virus-containing aerosols. Nevertheless, this work does offer important insights into the effect of heating on the charge. While heat seems to be suitable for PPE decontamination, detailed guidance on mask reuse is beyond the scope of this work. However, we refer the interested readers to CDC guidelines on this topic.[49]

MATERIALS AND METHODS

Materials. We selected three NIOSH-approved N95 respirators (1860, 8210, and 8511 from 3M) as well as four KN95 respirators. Two EUA-approved KN95 respirators (Guangzhou Powecom Labor and Zhejiang Lily Underwear Co. Ltd.) and two non-EUA-approved KN95 respirators (Supplyaid Rapid Response LLC and Henan Yomasi Health Technology, Inc.) were tested in this study (Figure S11A). N95 respirators (1860, 1870, and 8210 from 3M) sterilized by the VHP method were obtained from UCSD School of Medicine (San Diego, CA). N95 is NIOSH-approved with 95% filtration efficiency.[50] KN95 is GB 2626-2019-approved with 95% filtration efficiency.[51] We also studied surgical masks including face masks from Shandong Yushengyuan Medical Technology Co Ltd., cotton masks from Egyptian cotton face mask, and polyester masks and fabric face mask from Winwin.

https://dx.doi.org/10.1021/acsami.0c17333
ACS Appl. Mater. Interfaces XXXX, XXX, XXX−XXX

Sample Preparation. Pristine N95 and KN95 respirators were worn for 3 days. Each sample was cut into 2 cm × 2 cm pieces before putting it into the oven. After each cycle of the heat treatment, we used tweezers to transfer the samples into 50 mL conical centrifuge tubes to prevent contamination. We waited 15 min between treatment rounds. This allowed the sample to return to ambient temperature before being heated again.

Calculation of Pore-Area Size, Fiber Diameter, and Layer Thickness. SEM images were converted to black (pore) and white (MB fibers) to calculate pore-area size of the filter layer using Image J software[52] (Figure S3). The average diameter of 25 fibers in each layer was also calibrated using image J software. Digital calipers (Digimatic; Mitutoyo 500-505-10CERT) were used to measure the total thickness of the outer, filter, cotton, and inner layers in the respirators (Figure S11B).

Dry-Heat Treatment. A thermostat-controlled heating oven (T9FB2187511, ThermoFisher) was used for heat treatments. The interior size of the oven is 34.3 cm (length), 35.4 cm (width), and 50.8 cm (height) for 62 L of total volume. There were three shelves in the oven where respirators could be placed without stacking them together. Thus, it was capable of heating 18 respirators at once. The oven has a temperature range of up to 330 °C, and the fan in the oven maintains dry-heat condition. We conducted 150 °C treatment as a positive control because the recommended temperature for PP is 90 °C.[8]

Material Filtration Test. We used a PortaCount Plus Model 8020 respirator fit tester,[53] which measures the number of particles pre- and post filtration per cubic centimeter (cm^3) along with a fit factor. The instrument is best used in a closed room where the particle count is at least 30 000 particles per cm^3. Therefore, we conducted all of the measurements in the presence of two lit candles in a closed room; our goal was to maintain more than 50 000 particles per cm^3.[54−56]

For material filtration tests, N95 and KN95 respirators were cut into 2 cm squares and placed into a 2-cm-diameter cylindrical chamber. This chamber sealed the test sample in between two pieces of polycarbonate with inlet and outlet valves (see Figure S12). The inlet valve is sampled from the room air. The outlet value carried filtered air and passed into the PortaCount instrument (Figure S12D). The number of particles going into the PortaCount was measured for 30 s. The number of particles was also determined without filtration. The filtration efficiency of the sample was calculated using the following equation and was repeated 10 times to get an average value[57]

$$\text{material filtration efficiency} : \left(1 - \frac{\text{particle (per cm}^3\text{) not filtered}}{\text{particle (percm}^3\text{) in the ambient atmosphere}}\right) \times 100$$

The NIOSH method for measuring filtration efficiency uses sodium chloride (NaCl) aerosol with a count median diameter (CMD) of 0.075 ± 0.02 μm and a geometric standard deviation (GSD) of less than 1.86.[57] We did not have access to the NaCl aerosol and thus used the candle method described previously.[42,43] This approach creates ultrafine particles with a GMD of 0.02−0.03 μm and a GSD of 1.608. Thus, our approach generates smaller particles than the NIOSH method. Small droplets with a diameter below 0.8 μm are a major route of viral transmission,[58,59] and thus we are confident that the candle method has value in testing the filtration efficiency.

Electron Microscopy Imaging. A scanning electron microscope (SEM; FEI Apreo) was used to analyze structural information of SB and MB fibers in N95 and KN95 respirators. SEM images were taken at an accelerating voltage of 1 kV and a current of 0.10 nA. We took SEM images at the same spot of the outer layer after each cycle of heat treatment to test the progress of particle removal.

Dipole Charge Density. A Trek model 344 electrostatic voltmeter was used to measure the dipolar surface voltage of the filter layer. During the voltage measurement, one side of the filter layer was attached onto a grounded plate electrode, and a noncontact Kelvin probe was held 5 mm above the sample's top surface along its centerline to calculate the surface charge. We used the surface voltage results to calculate the corresponding surface charge densities. The dipole charges were determined by calculating the surface charge densities on the two sides of the sample. We previously used this exact instrument (Trek Model 344) for similar calculations.[60] We further validated the Trek Model 344 via controls with known charges such as polyethylene (PET) and paper: the results are comparable to prior work[61,62] (Table S2).

Isopropanol (IPA) Treatment. The filter layers of N95 and KN95 respirators were dipped into IPA solution for 30 s to remove all dipole charges. The samples were then dried at 35 °C in the air for 1 h.

■ ASSOCIATED CONTENT

Supporting Information

The Supporting Information is available free of charge at https://pubs.acs.org/doi/10.1021/acsami.0c17333.

Layer thickness of N95 and KN95 respirators; dipole charge density of PET and paper; fiber diameter of N95 and KN95 respirators; commonly available commercial masks; SEM images of each layer in N95 and KN95 respirators; fiber integrity of N95 and KN95 respirators after 150 °C treatment; a balloon-shaped fiber expansion in a KN95 respirator; SEM images of each layer after a filtration efficiency test; SEM images and thickness of N95 respirators after IPA treatment; dipole charge and filtration efficiency of KN95 after IPA treatment; SEM images and thickness of KN95s after IPA treatment; pore-area size measurement; material information and calibrator; filtration test of an N95 respirator; and fit factor (PDF)

■ AUTHOR INFORMATION

Corresponding Author

Jesse V. Jokerst − *Materials Science and Engineering Program, Department of Nanoengineering, and Department of Radiology, University of California San Diego, La Jolla, California 92093, United States;* orcid.org/0000-0003-2829-6408; Email: jjokerst@ucsd.edu

Authors

Wonjun Yim − *Materials Science and Engineering Program, University of California San Diego, La Jolla, California 92093, United States*

Diyi Cheng − *Materials Science and Engineering Program, University of California San Diego, La Jolla, California 92093, United States*

Shiv H. Patel − *School of Medicine Simulation Training Center and Division of Biological Sciences, University of California San Diego, La Jolla, California 92093, United States*

Rui Kou − *Department of Structural Engineering, University of California San Diego, La Jolla, California 92093, United States;* orcid.org/0000-0002-7370-6827

Ying Shirley Meng − *Materials Science and Engineering Program and Department of Nanoengineering, University of California San Diego, La Jolla, California 92093, United States*

Complete contact information is available at: https://pubs.acs.org/10.1021/acsami.0c17333

https://dx.doi.org/10.1021/acsami.0c17333
ACS Appl. Mater. Interfaces XXXX, XXX, XXX−XXX

Notes

The authors declare no competing financial interest.

■ ACKNOWLEDGMENTS

The authors acknowledge funding from the University of California Tobacco Related-Disease Research Program (TRDRP) under Emergency COVID-19 Research Seed Funding award number R00RG2515. The authors also acknowledge NIH under grants DP2 HL137187 and R21 AG065776 and NSF under grant no. 1845683 and NIH R21 AI157957. We acknowledge Bevis Respirator Consultants for the use of the PortaCount system. The authors also acknowledge our clinical collaborators, Dr. Benjamin Supat and Dr. Megan Tresenriter, for providing the respirators and support of VHP.

■ REFERENCES

(1) Baud, D.; Qi, X.; Nielsen-Saines, K.; Musso, D.; Pomar, L.; Favre, G. Real Estimates of Mortality Following COVID-19 Infection. *Lancet Infect. Dis.* **2020**, *20*, No. 773.

(2) Yan, R.; Zhang, Y.; Li, Y.; Xia, L.; Guo, Y.; Zhou, Q. Structural Basis for the Recognition of SARS-CoV-2 by Full-Length Human ACE2. *Science* **2020**, *367*, 1444−1448.

(3) Wang, J.; Du, G. COVID-19 may Transmit through Aerosol. *Ir. J. Med. Sci.* **2020**, *189*, 1143−1144.

(4) Prather, K. A.; Wang, C. C.; Schooley, R. T. Reducing Transmission of SARS-CoV-2. *Science* **2020**, *368*, 1422−1424.

(5) Patel, S. H.; Yim, W.; Garg, A. K.; Shah, S. H.; Jokerst, J. V.; Chao, D. L. Assessing the Physiological Relevance of Cough Simulators for Respiratory Droplet Dispersion. *J. Clin. Med.* **2020**, *9*, No. 3002.

(6) Qian, Y.; Willeke, K.; Grinshpun, S. A.; Donnelly, J.; Coffey, C. C. Performance of N95 Respirators: Filtration Efficiency for Airborne Microbial and Inert Particles. *Am. Ind. Hyg. Assoc. J.* **1998**, *59*, 128−132.

(7) Konda, A.; Prakash, A.; Moss, G. A.; Schmoldt, M.; Grant, G. D.; Guha, S. Aerosol Filtration Efficiency of Common Fabrics used in Respiratory Cloth Masks. *ACS Nano* **2020**, *14*, 6339−6347.

(8) Zerin, I.; Datta, E. A Review Article on Applications of Filter Cloth. *Int. J. Cloth. Sci.* **2018**, *5*, 1−6.

(9) Gobi, N.; Evangelin, S.; Kasthuri, R.; Nivetha, D. Multilayer Nonwoven Fabrics for Filtration of Micron and Submicron Particles. *J. Textile Eng. Fashion Technol.* **2019**, *5*, 81−84.

(10) Lam, T.-N.; Wu, C.-H.; Huang, S.-H.; Ko, W.-C.; Huang, Y.-L.; Ma, C.-Y.; Wang, C.-C.; Huang, E.-W. Multi-Scale Microstructure Investigation for a PM2. 5 Air-Filter Efficiency Study of Non-Woven Polypropylene. *Quantum Beam Sci.* **2019**, *3*, No. 20.

(11) Liu, J.; Zhang, X.; Zhang, H.; Zheng, L.; Huang, C.; Wu, H.; Wang, R.; Jin, X. Low Resistance Bicomponent Spunbond Materials for fresh Air Filtration with Ultra-High Dust Holding Capacity. *RSC Adv.* **2017**, *7*, 43879−43887.

(12) Dutton, K. C. Overview and Analysis of the Meltblown Process and Parameters *J. Text. Appar. Technol. Manag.* 2009, *6*, 1−24.

(13) Mukhopadhyay, A. Composite Nonwovens in Filters: Applications. In *Composite Non-Woven Materials*; Elsevier, 2014; pp 164−210.

(14) Grafe, T.; Graham, K. Polymeric Nanofibers and Nanofiber Webs: a New Class of Nonwovens. *Int. Nonwovens J.* **2003**, *12*, 1558925003os−12.

(15) Wang, C.-S. Electrostatic Forces in Fibrous Filters—a Review. *Powder Technol.* **2001**, *118*, 166−170.

(16) Pu, Y.; Zheng, J.; Chen, F.; Long, Y.; Wu, H.; Li, Q.; Yu, S.; Wang, X.; Ning, X. Preparation of Polypropylene Micro and Nanofibers by Electrostatic-Assisted Melt Blown and their Application. *Polymers* **2018**, *10*, No. 959.

(17) Matsuda, Y.; Saito, Y.; Tasaka, S. Dipole Polarization formed on Surface of Polypropylene Electrets. *IEEE Trans. Dielectr. Electr. Insul.* **2010**, *17*, 1015−1020.

(18) Kravtsov, A.; Brünig, H.; Zhandarov, S.; Beyreuther, R. The Electret Effect in Polypropylene Fibers Treated in a Corona Discharge. *Adv. Polym. Technol.* **2000**, *19*, 312−316.

(19) Brown, R. C. *Air Filtration: An Integrated Approach to the Theory and Applications of Fibrous Filters*; Pergamon, New York, 1993.

(20) Ranney, M. L.; Griffeth, V.; Jha, A. K. Critical Supply Shortages—the Need for Ventilators and Personal Protective Equipment during the Covid-19 Pandemic. *N. Engl. J. Med.* **2020**, *382*, No. e41.

(21) Ippolito, M.; Iozzo, P.; Gregoretti, C.; Cortegiani, A. Counterfeit Filtering Facepiece Respirators are Posing an Additional Risk to Healthcare Workers during COVID-19 Pandemic. *Am. J. Infect. Control* **2020**, *48*, 853−858.

(22) Fischer, R. J.; Morris, D. H.; van Doremalen, N.; Sarchette, S.; Matson, M. J.; Bushmaker, T.; Yinda, C. K.; Seifert, S. N.; Gamble, A.; Williamson, B. N.; Judson, S. D.; de Wit, E.; Lloyd-Smith, J. O.; Munster, V. J. Effectiveness of N95 Respirator Decontamination and Reuse against SARS-CoV-2 Virus. *Emerging Infect. Dis.* **2020**, *26*, 2253−2255.

(23) Mantri, Y.; Davidi, B.; Lemaster, J. E.; Hariri, A.; Jokerst, J. V. Iodide-doped precious Metal Nanoparticles: Measuring Oxidative Stress in vivo via Photoacoustic Imaging. *Nanoscale* **2020**, *12*, 10511−10520.

(24) Raeiszadeh, M.; Adeli, B. A Critical Review on Ultraviolet Disinfection Systems against COVID-19 Outbreak: Applicability, Validation, and Safety Considerations. *ACS Photonics* **2020**, *7*, 2941−2951.

(25) Sandle, T. *Biocontamination Control for Pharmaceuticals and Healthcare*; Academic Press, 2018.

(26) US Food and Drug Administration. *Final Report for the Bioquell Hydrogen Peroxide Vapor (HPV) Decontamination for Reuse of N95 Respirators*; White Oak, MD: FDA, 2016.

(27) Xiang, Y.; Song, Q.; Gu, W. Decontamination of Surgical Face Masks and N95 Respirators by Dry Heat Pasteurization for One Hour at 70 °C. *Am. J. Infect. Control* **2020**, *48*, 880−882.

(28) Liao, L.; Xiao, W.; Zhao, M.; Yu, X.; Wang, H.; Wang, Q.; Chu, S.; Cui, Y. Can N95 Respirators be reused after Disinfection? How many Times? *ACS Nano* **2020**, *14*, 6348−6356.

(29) Anderegg, L.; Meisenhelder, C.; Ngooi, C. O.; Liao, L.; Xiao, W.; Chu, S.; Cui, Y.; Doyle, J. M. A Scalable Method of Applying Heat and Humidity for Decontamination of N95 Respirators During the COVID-19 Crisis. *PLoS One* **2020**, *15*, No. e0234851.

(30) Juang, P. S. C.; Tsai, P. N95 Respirator Cleaning and Reuse Methods Proposed by the Inventor of the N95 Mask Material. *J. Emerg. Med.* **2020**, *58*, 817−820.

(31) Cai, C.; Floyd, E. L. Effects of Sterilization With Hydrogen Peroxide and Chlorine Dioxide on the Filtration Efficiency of N95, KN95, and Surgical Face Masks. *JAMA Netw. Open* **2020**, *3*, No. e2012099.

(32) Ippolito, M.; Vitale, F.; Accurso, G.; Iozzo, P.; Gregoretti, C.; Giarratano, A.; Cortegiani, A. Medical Masks and Respirators for the Protection of Healthcare Workers from SARS-CoV-2 and other Viruses. *Pulmonology* **2020**, *26*, 204−212.

(33) Lustig, S.; Biswakarma, J. J.; Rana, D.; Tilford, S. H.; Hu, W.; Su, M.; Rosenblatt, M. S. Effectiveness of Common Fabrics to Block Aqueous Aerosols of Virus-like Nanoparticles. *ACS Nano* **2020**, *14*, 7651−7658.

(34) Wakelyn, P. J.; Bertoniere, N. R.; French, A. D.; Thibodeaux, D. P.; Triplett, B. A.; Rousselle, M.-A.; Goynes, W. R., Jr; Edwards, J. V.; Hunter, L.; McAlister, D. D.; Gamble, G. R. *Cotton Fiber Chemistry and Technology*; CRC Press, 2006.

(35) Zhao, M.; Liao, L.; Xiao, W.; Yu, X.; Wang, H.; Wang, Q.; Lin, Y. L.; Kilinc-Balci, F. S.; Price, A.; Chu, L.; Chu, M. C.; Chu, S.; Cui, Y. Household Materials Selection for Homemade Cloth Face Coverings and their Filtration Efficiency Enhancement with Triboelectric Charging. *Nano Lett.* **2020**, *20*, 5544−5552.

https://dx.doi.org/10.1021/acsami.0c17333
ACS Appl. Mater. Interfaces XXXX, XXX, XXX−XXX

(36) Lee, K.; Liu, B. Theoretical Study of Aerosol Filtration by Fibrous Filters. *Aerosol Sci. Technol.* **1982**, *1*, 147−161.
(37) Zhu, M.; Han, J.; Wang, F.; Shao, W.; Xiong, R.; Zhang, Q.; Pan, H.; Yang, Y.; Samal, S. K.; Zhang, F.; Huang, C. Electrospun Nanofibers Membranes for effective Air Filtration. *Macromol. Mater. Eng.* **2017**, *302*, No. 1600353.
(38) Chin, A. W. H.; Poon, L. L. M. Stability of SARS-CoV-2 in Different Environmental Conditions−Authors' reply. *Lancet Microbe* **2020**, *1*, No. e146.
(39) Mostofi, R.; Wang, B.; Haghighat, F.; Bahloul, A.; Jaime, L. Performance of Mechanical Filters and Respirators for capturing Nanoparticles——Limitations and Future Direction. *Ind. Health* **2010**, *48*, 296−304.
(40) Kim, C. S.; Bao, L.; Okuyama, K.; Shimada, M.; Niinuma, H. Filtration Efficiency of a Fibrous Filter for Nanoparticles. *J. Nanopart. Res.* **2006**, *8*, 215−221.
(41) He, X.; Reponen, T.; McKay, R. T.; Grinshpun, S. A. Effect of Particle Size on the Performance of an N95 Filtering Facepiece Respirator and a Surgical Mask at Various Breathing Conditions. *Aerosol Sci. Technol.* **2013**, *47*, 1180−1187.
(42) Pagels, J.; Wierzbicka, A.; Nilsson, E.; Isaxon, C.; Dahl, A.; Gudmundsson, A.; Swietlicki, E.; Bohgard, M. Chemical Composition and Mass Emission Factors of Candle Smoke Particles. *J. Aerosol Sci.* **2009**, *40*, 193−208.
(43) Li, W.; Hopke, P. Initial Size Distributions and Hygroscopicity of Indoor Combustion Aerosol Particles. *Aerosol Sci. Technol.* **1993**, *19*, 305−316.
(44) Alison, J.; Hill, R. A Model for Bipolar Charge Transport, Trapping and Recombination in Degassed Crosslinked Polyethene. *J. Phys. D: Appl. Phys.* **1994**, *27*, 1291−1299.
(45) Baudoin, F.; Le Roy, S.; Teyssedre, G.; Laurent, C. Bipolar Charge Transport Model with Trapping and Recombination: an Analysis of the Current versus Applied Electric Field Characteristic in Steady State Conditions. *J. Phys. D: Appl. Phys.* **2008**, *41*, 025306−025316.
(46) Le Roy, S.; Teyssedre, G.; Laurent, C.; Montanari, G. C.; Palmieri, F. Description of Charge Transport in Polyethylene Using a Fluid Model with a Constant Mobility: Fitting Model and Experiments. *J. Phys. D: Appl. Phys.* **2006**, *39*, 1427−1436.
(47) Chen, L.; Shi, Q.; Sun, Y.; Nguyen, T.; Lee, C.; Soh, S. Controlling Surface Charge Generated by Contact Electrification: Strategies and Applications. *Adv. Mater.* **2018**, *30*, No. 1802405.
(48) Ohmi, T.; Sudoh, S.; Mishima, H. Static Charge Removal with IPA Solution. *IEEE Trans. Semicond. Manuf.* **1994**, *7*, 440−446.
(49) Planning, P. *Recommended Guidance for Extended Use and Limited Reuse of N95 FilteringFacepiece Respirators in Healthcare Settings*; US Government, 2020.
(50) Zhuang, Z.; Coffey, C. C.; Ann, R. B. The Effect of Subject Characteristics and Respirator Features on Respirator Fit. *J. Occup. Environ. Hyg.* **2005**, *2*, 641−649.
(51) Rubio-Romero, J. C.; del Carmen Pardo-Ferreira, M.; Torrecilla-García, J. A.; Calero-Castro, S. Disposable masks: Disinfection and Sterilization for Reuse, and Non-Certified Manufacturing, in the Face of Shortages during the COVID-19 Pandemic. *Saf. Sci.* **2020**, *129*, No. 104830.
(52) Rasband, W. *ImageJ*; US National Institutes of Health: Bethesda, Maryland, 1997.
(53) *Model 8095 N95−Companion to the PortaCount Plus. Operation and Service Manual*; TSI Inc. Shoreview: Minnesota, 2005.
(54) Kournikakis, B.; Harding, R. K.; Tremblay, J.; Simpson, M. Comparison of Protection Factors for selected Medical, Industrial and Military Masks. *J. Am. Biol. Saf. Assoc.* **2000**, *5*, 12−18.
(55) *PORTACOUNT Plus Model 8020 Operation and Service Manual*; TSI, Inc.: Minnesota, 2006.
(56) van der Sande, M.; Teunis, P.; Sabel, R. Professional and Home-Made Face Masks Reduce Exposure to Respiratory Infections among the General Population. *PLoS One* **2008**, *3*, No. e2618.
(57) Rengasamy, S.; Shaffer, R.; Williams, B.; Smit, S. A Comparison of Facemask and Respirator Filtration Test Methods. *J. Occup. Environ. Hyg.* **2017**, *14*, 92−103.
(58) Morawska, L.; Cao, J. Airborne Transmission of SARS-CoV-2: The World should face the Reality. *Environ. Int.* **2020**, *139*, No. 105730.
(59) Morawska, L.; Johnson, G.; Ristovski, Z.; Hargreaves, M.; Mengersen, K.; Corbett, S.; Chao, C. Y. H.; Li, Y.; Katoshevski, D. Size Distribution and Sites of Origin of Droplets expelled from the Human Respiratory Tract during Expiratory Activities. *J. Aerosol Sci.* **2009**, *40*, 256−269.
(60) Zhong, Y.; Kou, R.; Wang, M.; Qiao, Y. Electrification Mechanism of Corona Charged Organic Electrets. *J. Phys. D: Appl. Phys.* **2019**, *52*, No. 445303.
(61) Xu, Z.; Zhang, L.; Chen, G. Decay of Electric Charge on Corona Charged Polyethylene. *J. Phys. D: Appl. Phys.* **2007**, *40*, 7085−7089.
(62) Xu, Z.; Zhang, L.; Chen, G. In *Measurement and Analysis of Electric Potential Decay in Corona Charged Low-Density Polyethylene Films*, 2007 IEEE International Conference on Solid Dielectrics, IEEE, 2007; pp 454−457.

https://dx.doi.org/10.1021/acsami.0c17333
ACS Appl. Mater. Interfaces XXXX, XXX, XXX−XXX